Geophysical Research Letters

Supporting Information for

Unraveling the Source Locations of Short-Period Secondary Microseisms

Samuel Jorde[1,2], Martin Schimmel[1], Eleonore Stutzmann[3], Zongbo Xu[3,4], Pilar Sánchez-Pastor[1], Helena Seivane[1,5] and Jordi Díaz[1]

[1]Geosciences Barcelona (GEO3BCN), CSIC, Lluís Solé i Sabarís s/n, 08028 Barcelona, Spain

[2]Departament de Dinàmica de la Terra i de l'Oceà, Facultat de Ciències de la Terra, Universitat de Barcelona, Barcelona, Spain

[3]Université Paris Cité, Institut de physique du globe de Paris, CNRS, Paris, France

[4]Norwegian Geotechnical Institute, Oslo, Norway

[5]Observatorio Vulcanológico y Sismológico de Costa Rica (OVSICORI-UNA), Universidad Nacional, Costa Rica

Contents of this file

Text S1 to S2
Figures S1 to S8

Introduction

This supporting information provides additional details on the modelling and the SM pressure source PSDs, an explanation of how offshore source distances are derived from velocity attenuation, as well as several supplementary figures. Most of these figures show the results of the wave models during different source activation periods and the complementary wave heights corresponding to those shown in the paper.

Other figures include a comparison of attenuation across both broadband profiles, the distinct source distances obtained for each station, and the temporal consistency of secondary microseisms, separated into short- and long-period bands over multiple years. Back-azimuth estimates derived from the Rayleigh-wave polarization approach are also shown, revealing strong consistency through time. Finally, a figure with a representative example of the typical spectrum observed in NE Iberia is included showing the three main microseismic peaks.

Text S1.

For the modeling, we employ the algorithm from Xu et al. (2025) to model secondary microseism (SM) PSDs. This algorithm considers SM pressure source PSDs derived from WAVEWATCH III and Rayleigh wave propagation in weakly lateral-heterogeneous media (WLHM).

The WLHM Green's function is divided into three parts: source site coefficient, geometric and intrinsic attenuation, and receiver site coefficient. The source and receiver site coefficients are computed from CRUST1.0 model (Xu et al. 2025) whose spatial resolution is 1x1 deg. The resolution of the bathymetry map used in WW3 is 0.5x0.5 deg. Within each 1x1 deg. grid cell, four 0.5x0.5 deg. 1D models share one seismic model from CRUST1.0, while the ocean thickness varies according the bathymetry map. We use great-circle distance to compute the geometric attenuation, assuming that the Rayleigh waves in SM propagate along the great circles. To account for the intrinsic attenuation, we select an ad-hoc Q value from matching the synthetic and field SM observations. Note that this Q value of a station represents a spatial averaged Q among all the SM sources to the station, instead of a specific Rayleigh-wave propagation path. Further details about the modelling can be found in Xu et al. (2025).

In the SM pressure source PSDs, we have also included the SM excitation coefficients for Rayleigh waves (Longuet-Higgings, 1950; Ardhuin et al., 2011; Stutzmann et al., 2012; Gualtieri et al., 2013, among others), which are frequency- and bathymetry-dependent. With the grid resolution provided by WAVEWATCH III (0.5×0.5 deg.), we define the Mediterranean Sea as the study area and assume a crustal Vs of 2800 m/s. Iteratively, for each frequency in the 0.25–0.5 Hz range and for the bathymetry associated with each grid point, we estimate the excitation for each of the four tabulated modes proposed by Longuet-Higgings (1950) individually. We then sum their contributions to obtain the coefficient of the final response. Finally, we apply this coefficient to each frequency before integrating over the 0.25–0.5 Hz band to obtain the final SPSM pressure source maps considering the bathymetry.

Text S2.

Rayleigh wave amplitude decreases with distance due to both absorption and geometric spreading. In our case, the absorption effect is negligible along our profiles, therefore, we only use geometric spreading, which causes the amplitude to decay approximately as $r^{-1/2}$, where r is the distance to the source. This behavior arises from the cylindrical nature of surface wave propagation.

The measured amplitude $A(r)$ can thus be approximated as

$$A(r) \approx \frac{A_0}{\sqrt{r}}$$

where A_0 is the Rayleigh wave amplitude at the source together with all other constant factors. Comparing amplitudes in different stations we obtain:

$$\frac{A(r_i)}{A(r_j)} = \frac{\sqrt{r_i - \Delta r_{ij}}}{\sqrt{r_i}}$$

which can be rewritten as:

$$r_i = \frac{-\Delta r_{ij}}{\frac{A^2(r_i)}{A^2(r_j)} - 1}$$

where

$$\Delta r_{ij} = \cos\alpha \cdot D_{ij}$$

and where $A(r_i)$ and $A(r_j)$ represent the measured amplitudes at stations i and j, respectively, with i acting as the reference station; r_i is the distance between the source and station i; Δr_{ij} represents the difference in the distances from the source to stations i and j corrected from the source back-azimuth; α is the angle between the profile and the wavefront incidence direction; and D_{ij} is the distance between stations i and j. In our case, we assume a planar wavefront and a constant incidence angle at all stations along the profile. To make the approach more realistic, we select the central station as the reference station. Note that the negative sign of Δr_{ij} is only used when the station under consideration is closer to the source than the reference station, if it is farther from the source than the reference, the sign must be positive.

Then one day is selected, in this case August 3rd, 2024, which is one of the days with the highest attenuation and when the existence of a persistent source in the Mediterranean Sea is well known. The polarization analysis of this period highlights a clear maximum in the SPSM frequency band BAZ around 100° (Figure 3c). Velocity data for this day are acquired from all stations along the parallel profile. The data are then preprocessed by removing the trend, mean and the instrument response, and applying a band-pass filter between 0.25 and 0.5 Hz to isolate the SPSM band. The continuous data are then segmented into 30-minute traces. The time windows are not the same for all stations, as Rayleigh wave takes time to reach each station. Using a regional Rayleigh wave velocity of 2.5 km/s obtained from previous studies and correcting for an incidence angle of 100°, the windows are adapted for each station to allow comparison of equivalent time intervals. The mean amplitude of each time window is computed, and all stations are compared with the reference station. Angles of 95° and 105° are considered as α to encompass a wider range around the 100° BAZ maximum.

The results show that stations in the easternmost part of the profile exhibit consistent distances between 45–55 km (with around 15 km to the shoreline, resulting therefore in

30–40 km offshore), while stations in the westernmost part display negative distances. Negative values arise because the amplitude is higher at stations theoretically farther from the source than the reference station, suggesting a shift in the main source's influence along the profile. The primary source predominantly affects 4–5 stations in the eastern section, which are used to estimate the source distance (Figure S1), as these stations are less influenced by a secondary source located to the south. These observations further support the identification of distinct attenuation patterns associated with different predominant sources (Figure 3c), which appear to be active simultaneously in the Mediterranean.

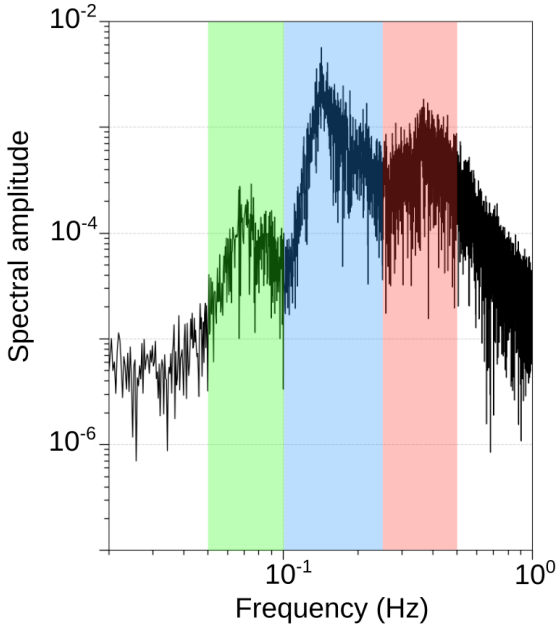


Figure S1. Typical spectrum recorded in NE Iberia showing the three frequency bands used in this study: PM (0.05 – 0.1 Hz), LPSM (0.1 – 0.25 Hz) and SPSM (0.25 – 0.5 Hz).

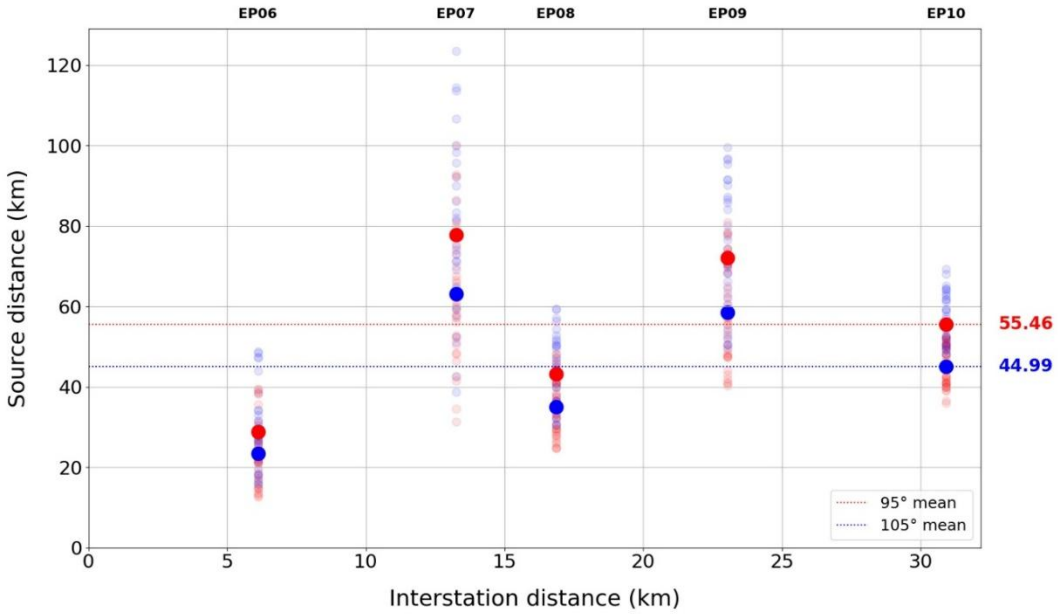


Figure S2. Mean source distances derived from the five easternmost stations of the parallel profile, for wavefront incident angles of 95° (red) and 105° (blue).

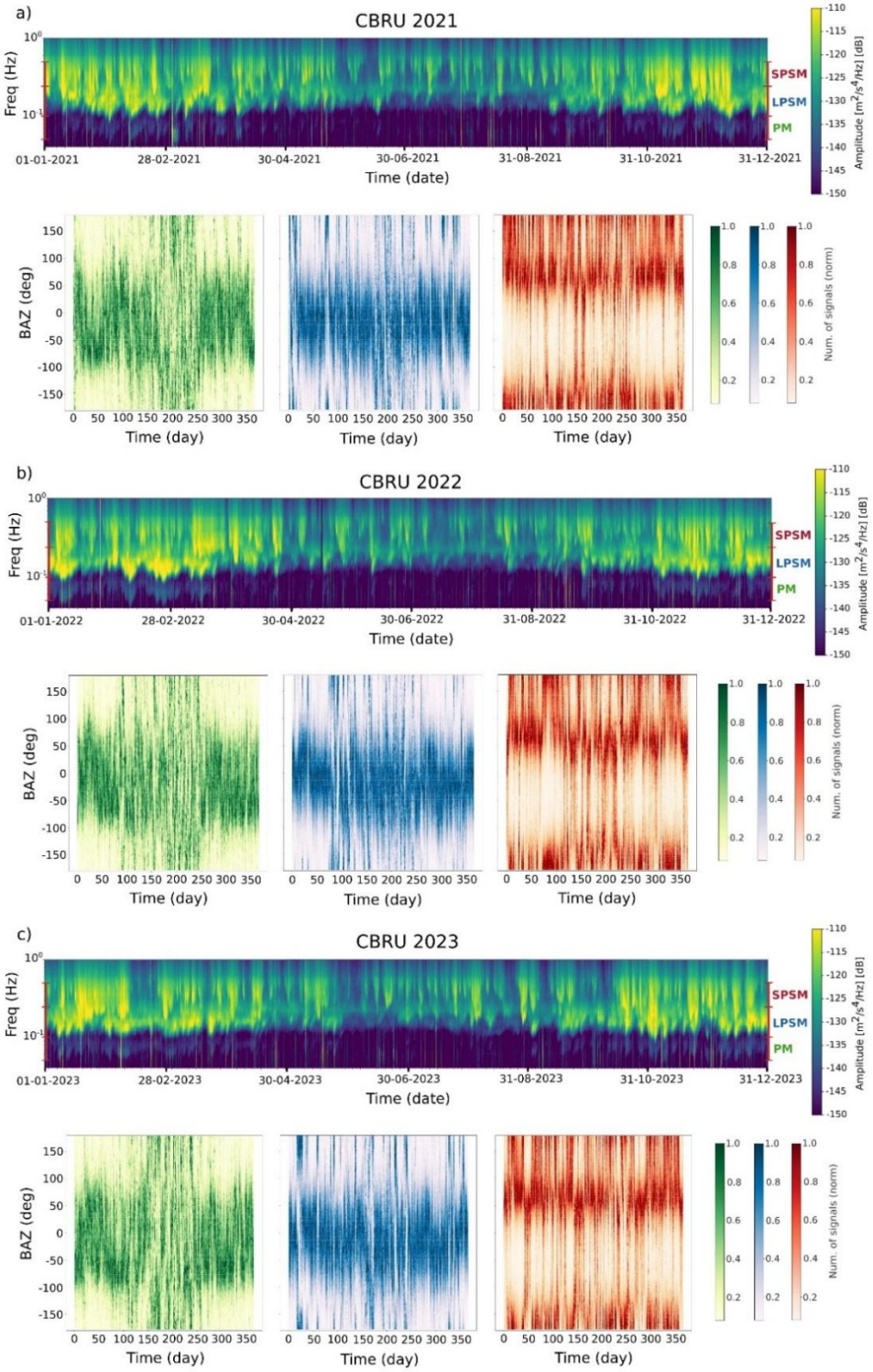


Figure S3. Annual spectrogram between 0.04 and 1 Hz for the CBRU permanent station, highlighting the frequency ranges of the microseisms: 0.05–0.1 Hz (PM), 0.1–0.25 Hz (LPSM), and 0.25–0.5 Hz (SPSM). The normalized number of elliptically polarized signals obtained for each microseism are also shown as a function of BAZ and time: PM (green), LPSM (blue), and SPSM (red). This is shown for 2021 (a), 2022 (b), and 2023 (c).

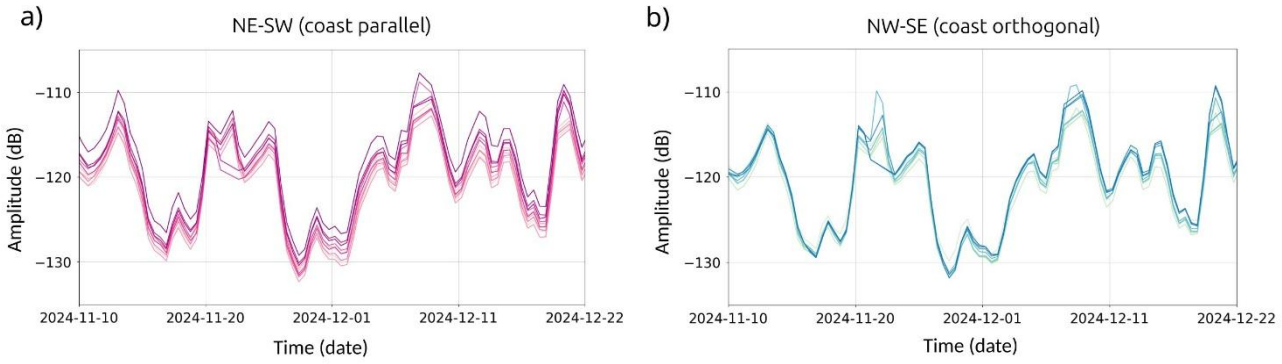


Figure S4. Amplitude attenuation across stations along the parallel (a) and orthogonal (b) profiles over two months (November–December 2024) in the 0.25– 0.5 Hz band.

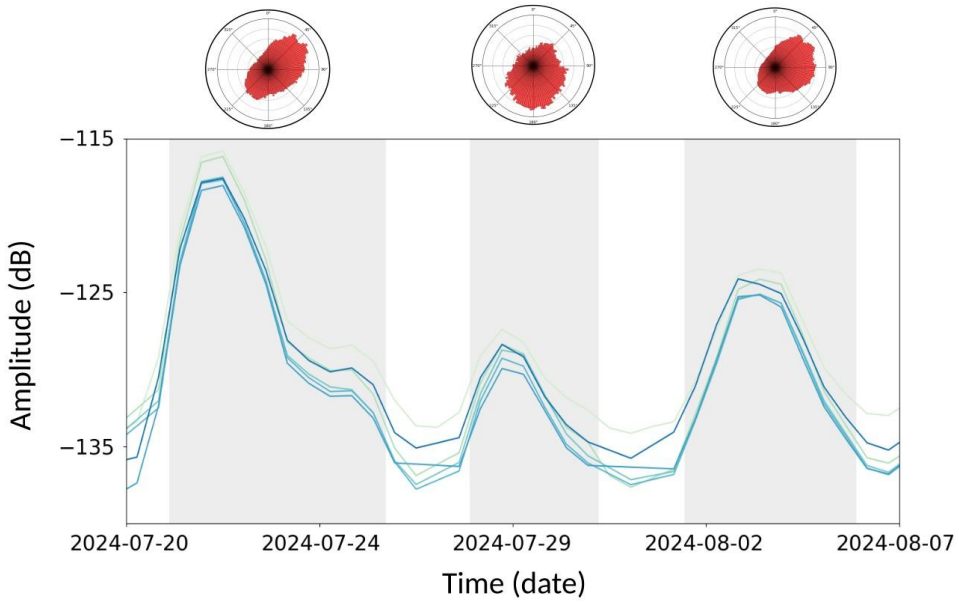


Figure S5. 18 days from the orthogonal profile, highlighting the two typical attenuation patterns and the corresponding BAZs derived from Rayleigh-wave polarization for the nearest station to the shoreline within the shaded areas.

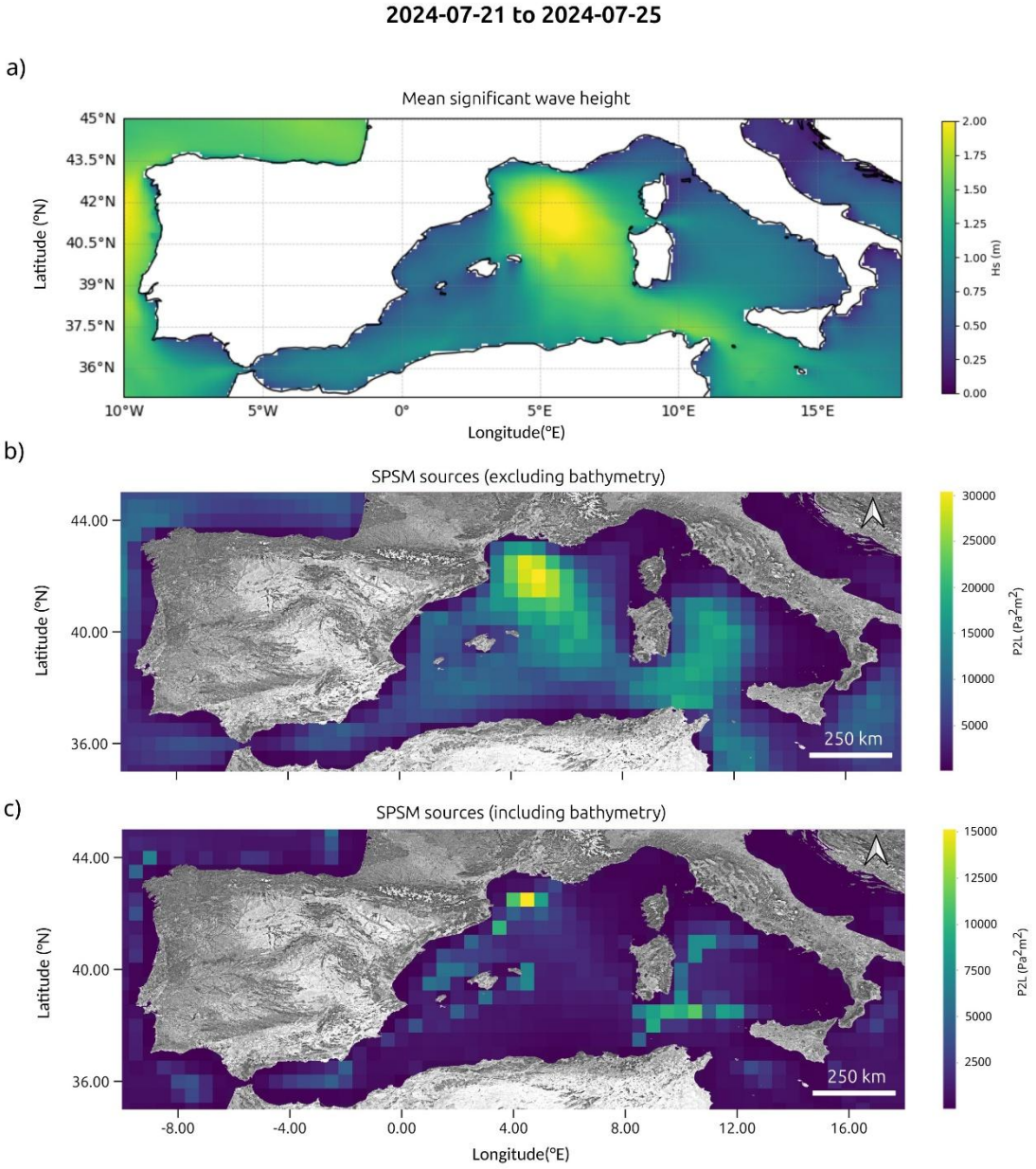


Figure S6. Wave models of the first source activation in Figure 3a. a) Mean significant wave height of the analysed period. b) SM pressure source PSD map integrated in time and frequency (0.25–0.5 Hz) excluding the bathymetry-dependent SM excitation coefficient. c) Same as (b) but considering the bathymetry.

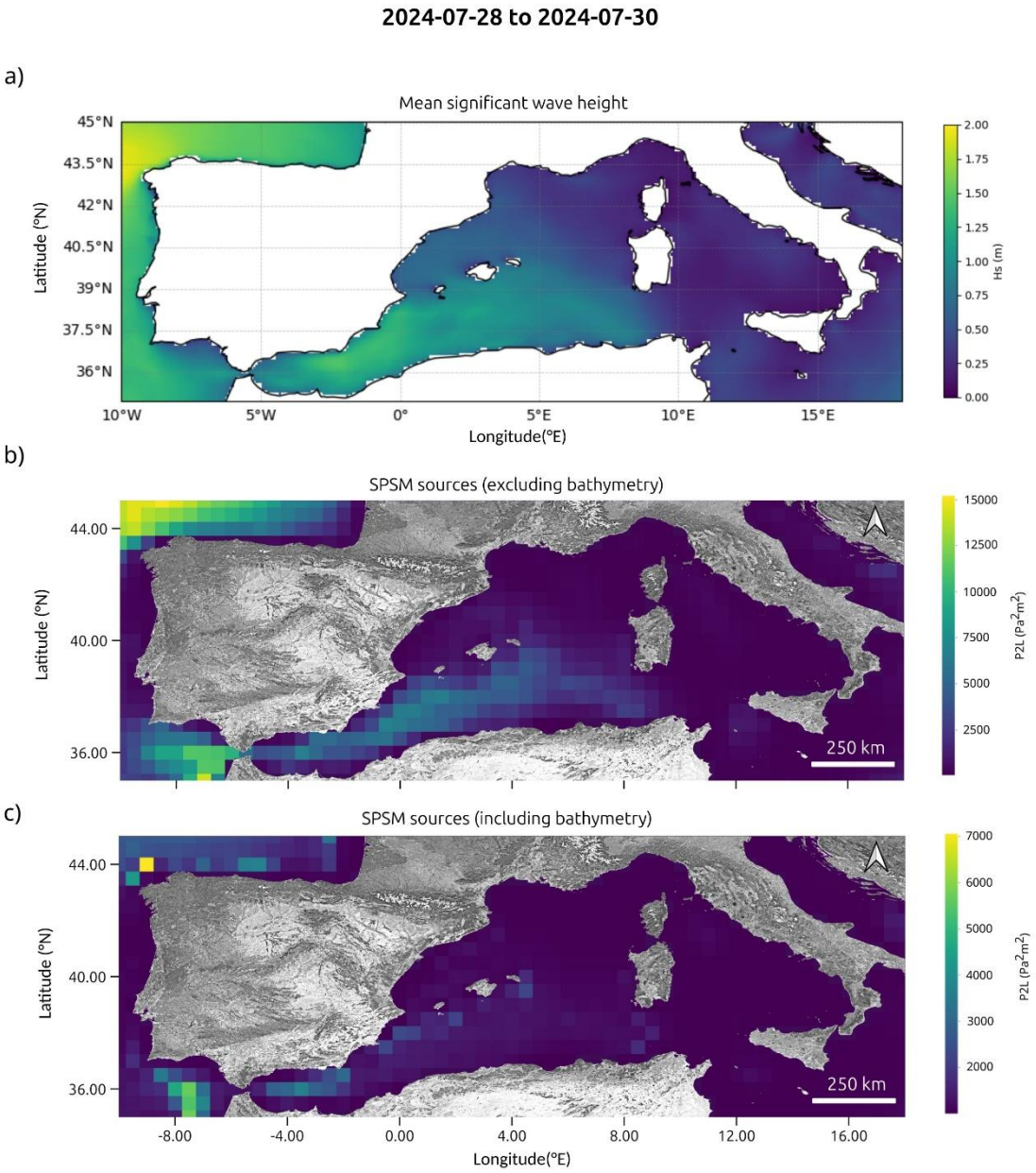


Figure S7. Wave models of the second source activation in Figure 3a. a) Mean significant wave height of the analysed period. b) SM pressure source PSD map integrated in time and frequency (0.25–0.5 Hz) excluding the bathymetry-dependent SM excitation coefficient. c) Same as (b) but considering the bathymetry.

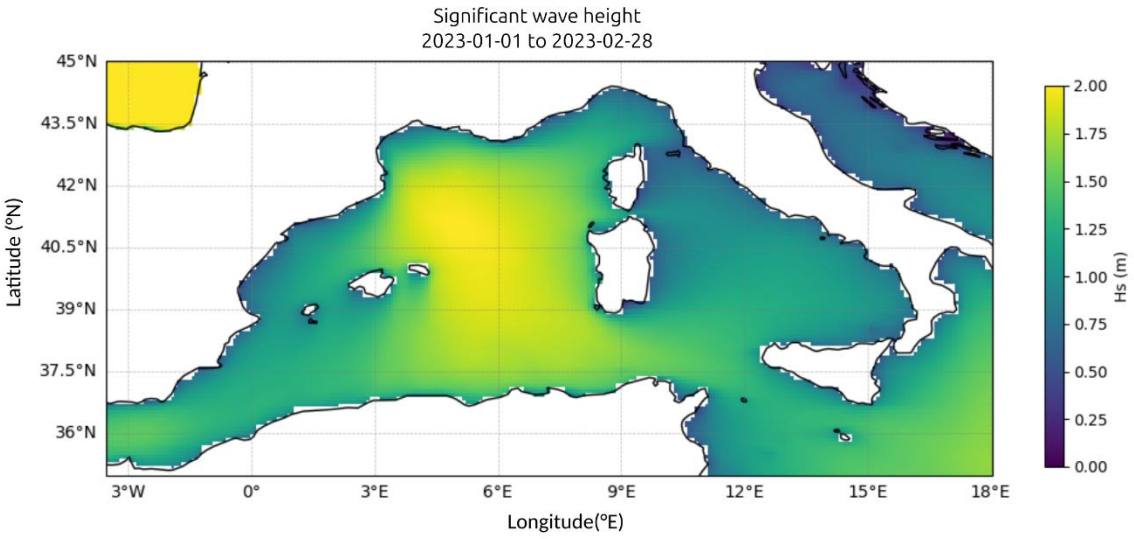


Figure S8. Mean significant wave height for the first two months of 2023.